ISSN No:-2456-2165

Tandem Analysis Effects on Bluff Bodies Aerodynamics

Mohammad Salem Alsubaiei[1]
[1]Eng., Specialist Trainer (B) in Public Authority for Applied Education and Training, the University of Arab Academy For Science, Technology & Maritime Transport

Saad Abdullah Alshatti[2*]
[2]Eng., Specialist Trainer (C) in Public Authority for Applied Education and Training, the University of Arab Academy For Science, Technology & Maritime Transport

Corresponding Author:- Saad Abdullah Alshatti[2*]

Abstract:- Flow over the bluff body is considered an interesting topic that has long piqued the curiosity of aerodynamic experts because of its unusual flow behavior. Moreover, bluff bodies used in tandem have several technical applications, including high tower buildings, railways trains, industrial chimneys, and road vehicles, in addition to several other applications. Nevertheless, the non-streamed bodies with sharp leading ends are subjected to very high-pressure drag. Recognizing the flow through these bodies contributed to the design optimization and management of the field using passive or active techniques. Hence, the primary goal of this research is to quantitatively explain the flow field and effect of shielding of different square plates positioned concentrically as front bodies square flat-faced upstream sharp leading edges in addition to the rounded back rear body. Furthermore, this study considered a 3D analysis of the fluid flow behavior near the rear body alone, considering various geometrical combinations of gap ratios and width. Also, this study involves three Reynolds numbers depending on the rear body width, which is in the range of 1-1.8 ×105 were considered. Results were obtained using ANSYS-FLUENT (19.1) software depending on Computational-Fluid-Dynamic (CFD) applied to the K-Ɛ turbulence model to solve the general equations and, therefore, test the prepared models. The flow properties were simulated, involving the components of flow stream velocity, pressure distribution, and the Pressure-Coefficient (Cp) of the front-rear body and near the rear body alone combinations. Results showed that the most effective combination is achieved when the g/b2 value equals 0.5 b1/b2 value equals 0.75. These parameters achieved a high drag reduction since the maximum value was 48% when the speed was 15m/s, as well as a drag reduction of 12% when the speed value was 20 m/s. This decrease is because of the impact of the front body's shielding, which causes separation streamlining on the front body's reattachment close to the shoulder of the rear body. Moreover, the instantaneous streamline velocity contour, as well as drag coefficient distributions, were computed. The obtained numerical results showed a good agreement with the experimental outcomes.

Keywords:- *Bluff Body, Computational-Fluid-Dynamic, ANSYS-FLUENT, Fluid Flow Behavior, Body's Shielding, Pressure-Coefficient (Cp).*

I. INTRODUCTION

A. Background

Bluff body term is commonly used in the aerodynamics field. It is a body with L/D ≤ 1.0 (L/D (Length/to/height), which means that the length with flow direction is around the length of the perpendicular to flow, where the flow is determined by flow coalescence, boundary layer separation, and the formation of eddies that feed into the wake zone around the body (Konstantinidis & Bouris, 2012). Figure 1 is a general explanation for the flow around a bluff body.

High pressure is applied at the front bluff body face, whereas low pressure is applied at the other three faces. This pressure difference leads to high-pressure drag. These flow properties are critical in the analysis of numerous applications. Moreover, flow over a bluff body has recently become a highly significant and intriguing issue, attracting the aerodynamic expert's attention because of their unusual flow behavior (Imron et al., 2013).

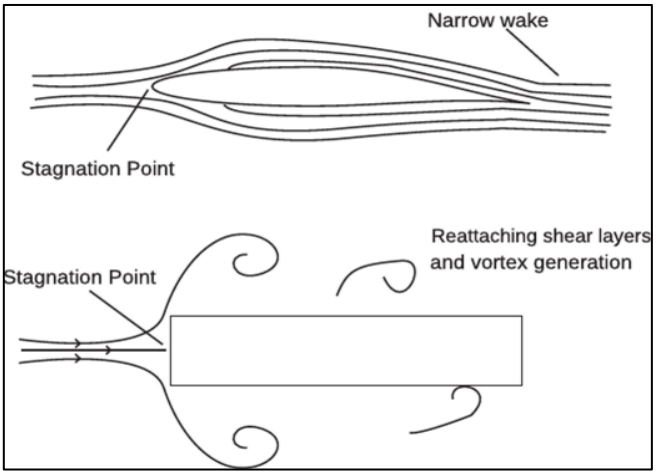

Fig 1 The flow Around a Bluff Body (Imron et al., 2013).

There are several engineering applications for tandem bluff bodies, including road automobiles, trains, tower buildings, as well as industrial chimneys. Furthermore, flow through these bodies help enhance the control and design of the flow field, utilizing passive and active techniques. The total drag force that affects the bodies in flow represents the total pressure drag as well as friction drag forces (Chen et

ISSN No:-2456-2165

al., 2020). Streamline bodies have connected flow. Hence, the drag is caused by shear stresses, while pressure drag is generally minor. However, the bluff body is subjected to pressure drag resulting from the force's normal distribution to the surface (Bao et al., 2022); this pressure drag can be thought of as the summation of three separate components, namely:

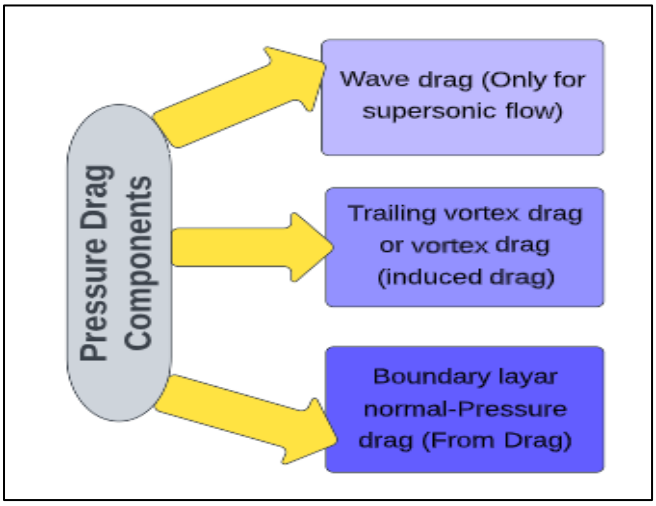

Fig 2 Pressure Drag Components

The separation of the boundary layer produces pressure drag. The drag force is preserved at the minimum amount for approximately all operation periods, not continuously. Power expenditure is needed to overwhelm the body in several ways. The drag forces. The drag force can be calculated using numerical techniques or by experimenting. Experimental studies have become a significant field in various research and led to several discoveries. However, compared to numerical techniques, these investigations require much cost and time.

Because of the developments in numerical analysis and computer technology, particularly the Computational-Fluid-Dynamic, symboled by (CFD), technology developed a more influential tool in handling the complications that include fluid flows. However, numerous investigations are solving and analyzing the reduction of drag force in addition to the flow field earlier in the bodies of 3D bluff by conducting experimental and numerical studies.

Sajali et al. (2021) conducted experiments analyzing the impact of square and D-shapes plat when the front body is positioned upstream at the square flat face, and the back body has sharp corners. It observed a significant drag reduction for specific combinations, precisely the gap and width ratios. Talele et al. (2021) analyzed the impact of several simulation parameters, such as turbulence model and mesh quality, arranged the unstable flow over the rectangular cylinder, and employed 2D and 3D models. Also, (Chen et al., 2022) analyzed in a numerical way the flow characteristics, for example, the transition and vortices spin of a square cylinder. Mathematical findings revealed that the change happened with Reynolds number among 150 in addition to 175.

Moreover, Li et al. (Li et al., 2021) Analysed the flow performance across radial rectangular, rectangular, and bullet-shaped using (CFD) technology. The research implies that the shaped body of the bullet is like a streamlined shape and that it is aerodynamically good quality compared to the whole additional cases. According to (Afifi et al., 2021), a study was prepared to investigate the body motion in fluid flows when changing the splitter plate length. The research examined the pressure as well as Mach number impacts on the body's surface. Also, it was critical to investigate fluid flows at more incredible speeds. A two-dimensional, rectangular shape bluff-body has a (50mm*60mm) controller for a splitter plate, which is evaluated utilizing a rectangular fluid domain—also, the splitter plate is situated at the body's front face to achieve a mechanism of a passive mechanism of control. The splitter plate parametric impact on the body height is also studied further in this work. Due to the incompressibility, the simulation ANSYS Fluent software was utilized to simulate the obtained results using a pressure-based solver. Furthermore, the simulation process was achieved depending on the k-e turbulent model; these results were confirmed using wind as the experimental outcome. Depending on the latest findings, it has been determined that the proposed model can be effectively used to examine fluid flow across the bluff body. Furthermore, the simulations' results show that the splitter plate critically influences the flows' separation from the turbulent flow. These results emphasized the benefits of using a splitter plate in the flow separating, reducing drag.

According to (Aabid et al., 2021), this research aims to look at the splitter plate's impact on controlling the bluff body's wake. The splitter plate is placed at the front of the analyzed rectangular bluff body depending on the passive control approach. Furthermore, the size of this body is (50 × 60) mm. Furthermore, the splitter plate length was examined regarding the height of the bluff-body. The K-epsilon-developed wall treatments turbulence model was employed in this work to validate simulation outcomes with the involved experimental data. Moreover, the experimental outcomes correlate with the simulation outcomes. Also, the upstream splitter plate considerably influences the turbulent flow drag reduction. Based on the outcomes, the analyzed splitter plate is beneficial for reducing drag by regulating the flow field.

- *Aims and Objectives*

The main aim of this paper is to analyze the Tandem Effects on Bluff Bodies Aerodynamics. Also, the paper aims to discover the numerical effect of several geometrical parameters, including gap ratio and width, on flow field behavior and drag for 2-bluff bodies (front & rear), which are disconnected by a gab within 3- various velocities. This study was conducted for 2- prominent cases: the rear body alone, in addition to a rear body connected with a square plate to act as a configuration of the front body. Certain combinations are responsible for determining the optimum combination, which results in a notable reduction in drag.

ISSN No:-2456-2165

II. METHODOLOGY

A. *Overview*

The methodology followed to achieve this work focused on selecting the suitable model, then identifying the data and collecting the data dimensions from the selected model (Khalid & Rathakrishnan, 1996). In this paper, two models were prepared, as illustrated in Figure 3.

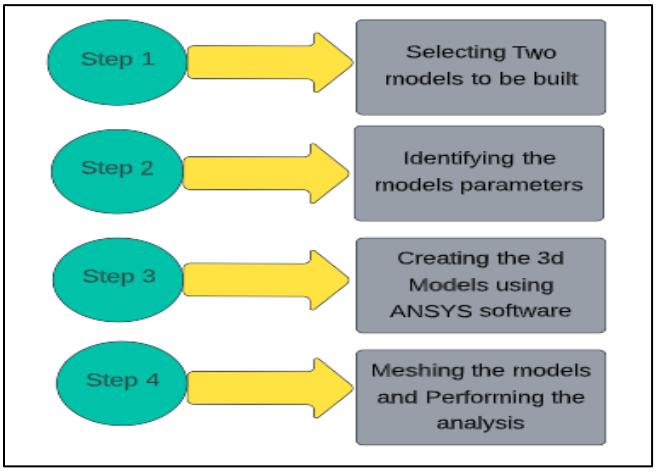

Fig 3 Methodology Steps

The first model in this research was D-shaped (rear-body). The dimension of this model was R (radius of curvature) =50 mm, b2 (width) = 100 mm). The second model in this research was the modified rear body with various ratios for width (b1/b2= 0.25, 0.37, 0.5, 0.625, 0.75, and 1.0). The parameter "g" represents the extended arm which holds the forward square plate which has a radius of "b1", where the entire entre-extended arm which based on the model bluff-body, which is based at "b2", the interval for the gab ratio (g/b2= 0.25, 0.5, 0.75. 1.0). The ANSYS software was used to create a 3D-model. As well, the generation of the final mesh depends on using 3D-element.

B. *Mathematical Models*

FLUENT ANSYS is commercial simulation software that analyses fluid motion based on the ANSYS workbench. Fluent ANSYS can be applied in several advanced physics, such as mechanical and thermal investigations of electrical motors. This software includes all essential tools to model aerodynamic applications, heat transfer, and fluid flow. The 3D model utilized in this study uses the k-ε turbulence model. In the present work, the domain length and width are suggested by (Malizia et al., 2016) to acquire accurate and reliable outcomes. The boundary conditions and computational domain utilized in the current study are offered in Figure 4.

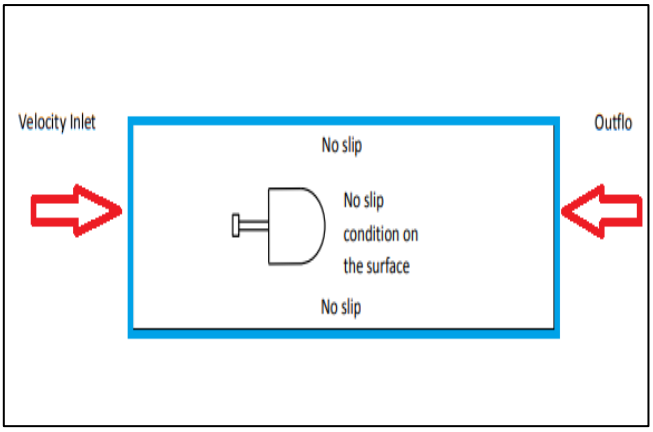

Fig 4 Boundary Conditions and Computational Domain (Malizia et al., 2016)

It mainly consists of three regions. Zone one denotes the inlet flow condition and is designed as inlet velocity with three significant values, 15 m/s, 20m/s, and 26 m/s. Region two denotes the walls of the wind tunnel and bluff-body, and both are deemed as the walls of no-slip stationery. Region three, the rear boundary, determines the pressure outlet identical to the turbulence specification with zero-gauge pressure.

C. *Meshing Process*

This study evaluated a 3D airflow near the various rear bodies and bluff combination for different gap ratios b1/b2 and g/b2 at different velocities of 15 m/s, 20 m/s, and 26 m/s employing FLUENT ANSYS 19.2. Meshing tools in the Ansys are utilized to bring the meshing. The mesh details are given by: Utilize adaptive sizing (yes), Transition (slow), Resolution (7), smoothing (medium), Span angle (Fine), Nodes (81723), elements (451531), Maximum (5), and Transition ration (0.272). Figure 5 represents the boundary conditions and computational domain modeling.

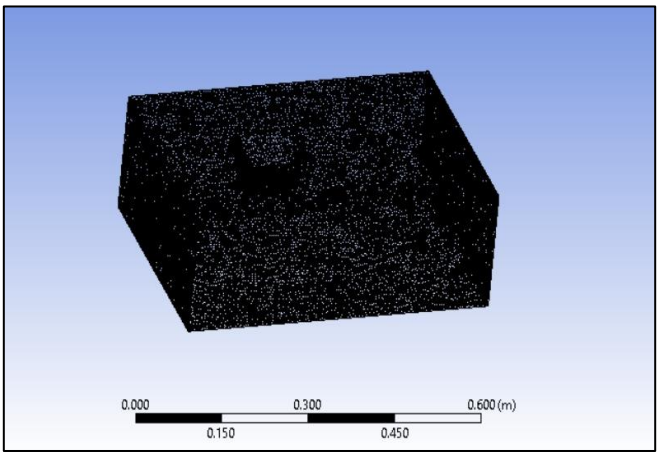

Fig 5 Boundary Conditions and Computational Domain Modeling

ISSN No:-2456-2165

The ANSYS software solves the equation of continuity and incompressible Navier-Stokes as given:

$$\frac{d\bar{u}_i}{dx_i} = 0$$

$$\frac{d\bar{u}_i}{dx_i} + \frac{d\bar{u}_i\,\bar{u}_j}{dx_j} = \frac{1}{p}\frac{d\bar{p}}{dx_i} - \frac{d\left(\bar{u}_i\,\bar{u}_j - \bar{u}_i\,\bar{u}_j\right)}{dx_i} + V\frac{d^2\bar{u}_i}{dx_i dx_j}$$

Where u_i represents the velocity components, x_i denotes the Cartesian coordinates, t represents the time, and v refers to the kinematic viscosity. Therefore, to solve the equation of Navier-Stokes motion and the equation of continuity, the method of finite volume is utilized and is expressed as (Yagmur et al., 2015):

$$\int\left(\int_t^{t+\Delta t}\frac{d}{dt}(\rho\emptyset)dt\right) + \int_t^{t+\Delta t}\left(\int n(\rho u\phi)dA\right)dt = \int_t^{t+\Delta t}\left(\int n(\Gamma\,\mathrm{grad}\phi)\;dA\right)\;dt + \int_t^{t+\Delta t}\left(\int S_\phi\,dV\right)dt$$

$$\int\left(\int_t^{t+\Delta t}\frac{d}{dt}\;(\rho\phi)dt\right) + \int_t^{t+\Delta t}\left(\int n(\rho u\phi)dA\right)dt =$$

$$\int_t^{t+\Delta t}\left(\int n(\Gamma\,\mathrm{grad}\phi)dA\right)dt + \int_t^{t+\Delta t}\left(\int S_\phi dV\right)dt$$

Where ϕ refers to the growth rate and general property, Γrefers to the diffusion coefficient. The drag coefficient or C_d parameter can be discovered as follows:

$$C_d = \frac{\text{Drag Force}}{0.5 \times \rho \times A \times V^2}$$

III. RESULTS AND DISCUSSION

ANSYS/FLUENT was used for numerically solving equations 1, 2, and 3 under the given boundary conditions. The results concentrated on covering the flow around the rear body alone model and the combinations of the front-rear body (six and four width and gap ratios, respectively) based on the free-stream velocities values (15 m/s,20 m/s, and 26 m/s). To achieve the aim of this research, the data are calculated to be compared and discussed based on the other computed data and the experimentally evaluated data.

A. Rear Body Alone Results

The location of the contoured column lies on the left side, representing the numerical stream velocity. The orange area represents all the stream velocities. Blue and red colors, respectively, represent the slow and high velocities. Increasing the free stream velocity occurs due to increasing the pressure drag. These results are included in the wake zone located in the rear body part, as noted in the contours of the stream velocity, as represented in Figures 6 (a), (b), and (c).

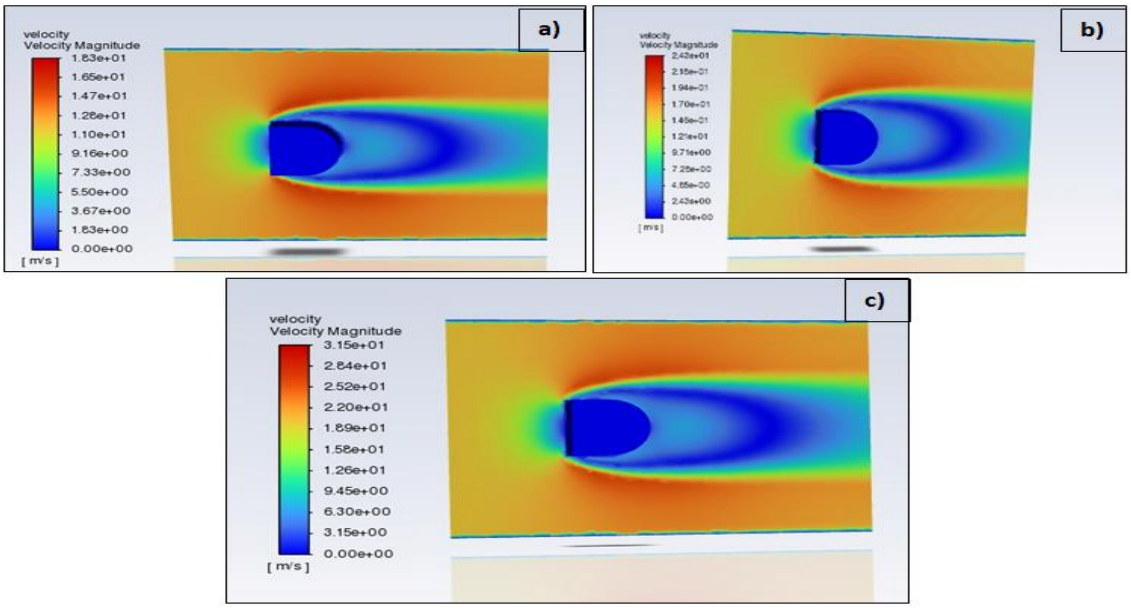

Fig 6 Velocity for Different Velocity Values (15, 20, 26 m/s)

ISSN No:-2456-2165

The rear body's front edges experience separation on the boundaries of the layers. Eddies strongly and alternatively feed these edges. Accordingly, a high wake zone will be produced behind the body with a high drag coefficient value. The pressure coefficient is represented on the right side of Figures 7 (a), (b), and (c) for three different velocity values. The red area indicates the high positive pressure values. Such excess pressure occurs because the approaching flow stagnates on the front face of the rear body. However, the high negative pressure values are indicated by the blue area. This suction pressure happens as the boundary layers separate at the sharp corners.

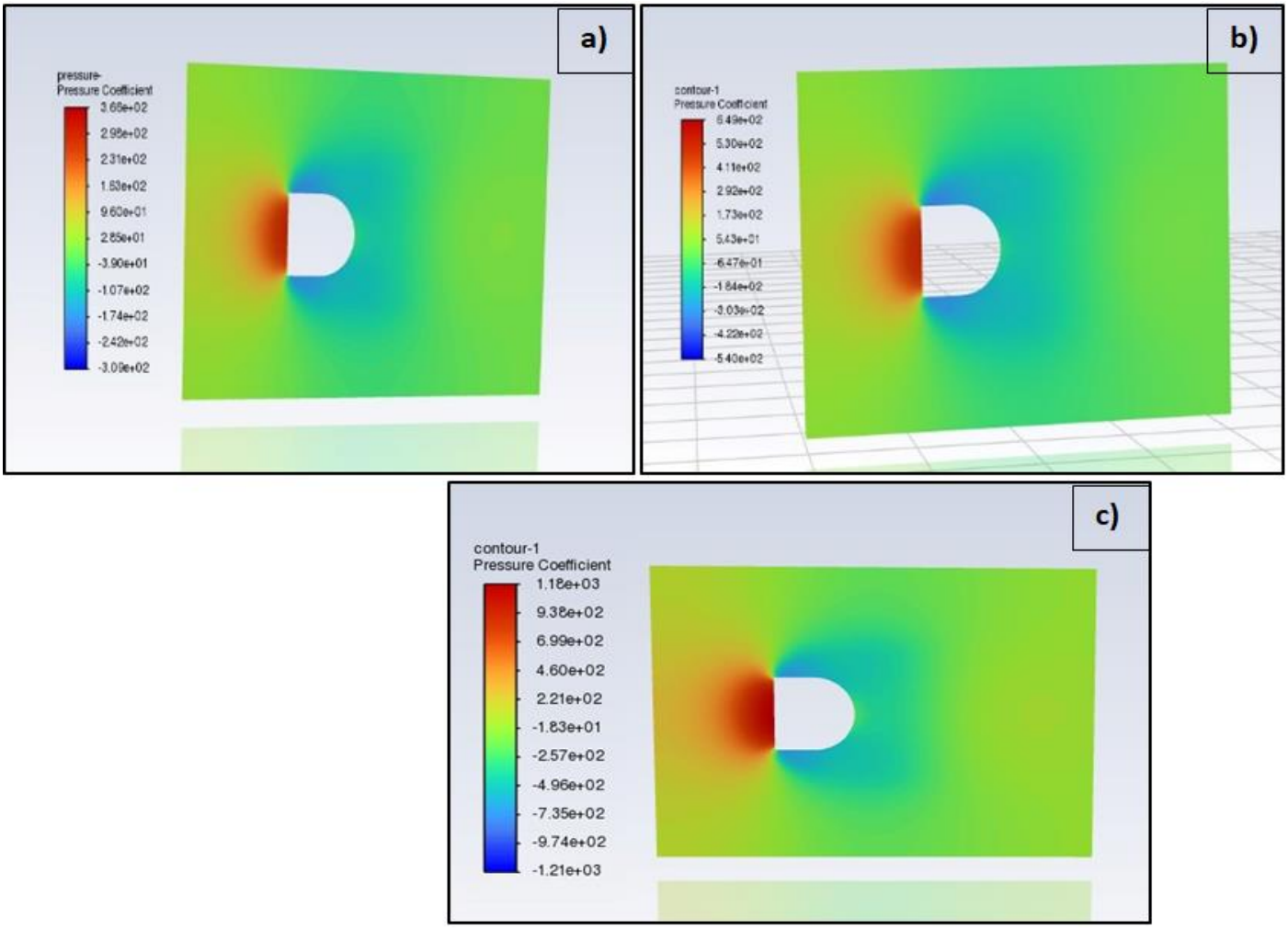

Fig 7 Pressure Contours for Different Velocity Values (15, 20, 26 M/S) for the Rear Body Only

Accordingly, the drag pressure is the difference value between the suction and excess pressure. The CDO values corresponding to the velocity values are (1.213 for $V_1 = 15\ \frac{m}{s}$, 1.214 for $V_2 = 20\ \frac{m}{s}$, and 1.216 for $V_3 = 26\ \frac{m}{s}$). Additionally, the experimental outcomes were matched with the numerical results for the drag coefficient of the rear body, as represented in Table 1. As shown, the error percentage between both results is 5%, 12%, and 14% for the velocities $15\ \frac{m}{s}$, $20\ \frac{m}{s}$, and $26\ \frac{m}{s}$, respectively.

B. Front-Rear Body Combinations Results

The stream velocity variation for the combination of the front-rear body, when geometry such as width ratios are existed $(b_1 / b_2 = 0.25, 0.37, 0.50, 0.62, 0.75 \text{ and } 1.0)$ and $g / b_2 = 0.5$ at velocity $15\ m/s$. Figure 8 represents the effect of the width ratio on the wake zone and the stream velocity. The red area represents the low value of pressure and the high value of velocity values. In contrast, the high-pressure and the low-velocity values are represented in the blue area. The optimal combination is distinguished by (*).

Figure 8 (a) represents the small width value (0.25). The boundary layer split from the front body is re-attached to the rear face of the body. Then, it will separate from the rear corners of the body. A high drag coefficient value with an opened wake zone has resulted since the wake zone is initiated approximately on the shoulders. When the width ratio is 0.37, a flow similar to that obtained in the 0.25 ratio is noticed. However, there is a tendency to separate boundary layers from the front body to re-attach with the rear body shoulders. A smaller wake zone has resulted than this obtained when the width ratio equals 0.25. The width ratios are 0.5 and 0.62, represented in Figures 8 (c) and (d), are similar to the optimal case ($\frac{b_1^*}{b_2}$ and $\frac{g^*}{b_2}$ equals 0.75 and 0.5, respectively) presented in Figure 8 (e). The rear body shoulders and the separated boundary layers are relatively close. However, the separated layers show unsteadiness.

ISSN No:-2456-2165

When the width ratio is 0.75, as represented in Figure 8 (e), a steady flow is noticed, and the boundary layers that are split from the front body are thin so that a reattachment will happen at the shoulder of the rear body. Accordingly, a good effect of shielding has resulted. The optimum case is noticed when ($\frac{b_1^*}{b_2} = 075$ and $\frac{g^*}{b_2} = 0.5$). In this case, a minimum value of CD = 0.604 is noticed, which is smaller than the C_D coefficient by approximately 48% for the rear body alone. Figure 8 (f) represents the results obtained when the width ratio is 1.0, in which the separated layers have existed on the rear body sides. Therefore, the drag coefficient is higher than those obtained by other combinations.

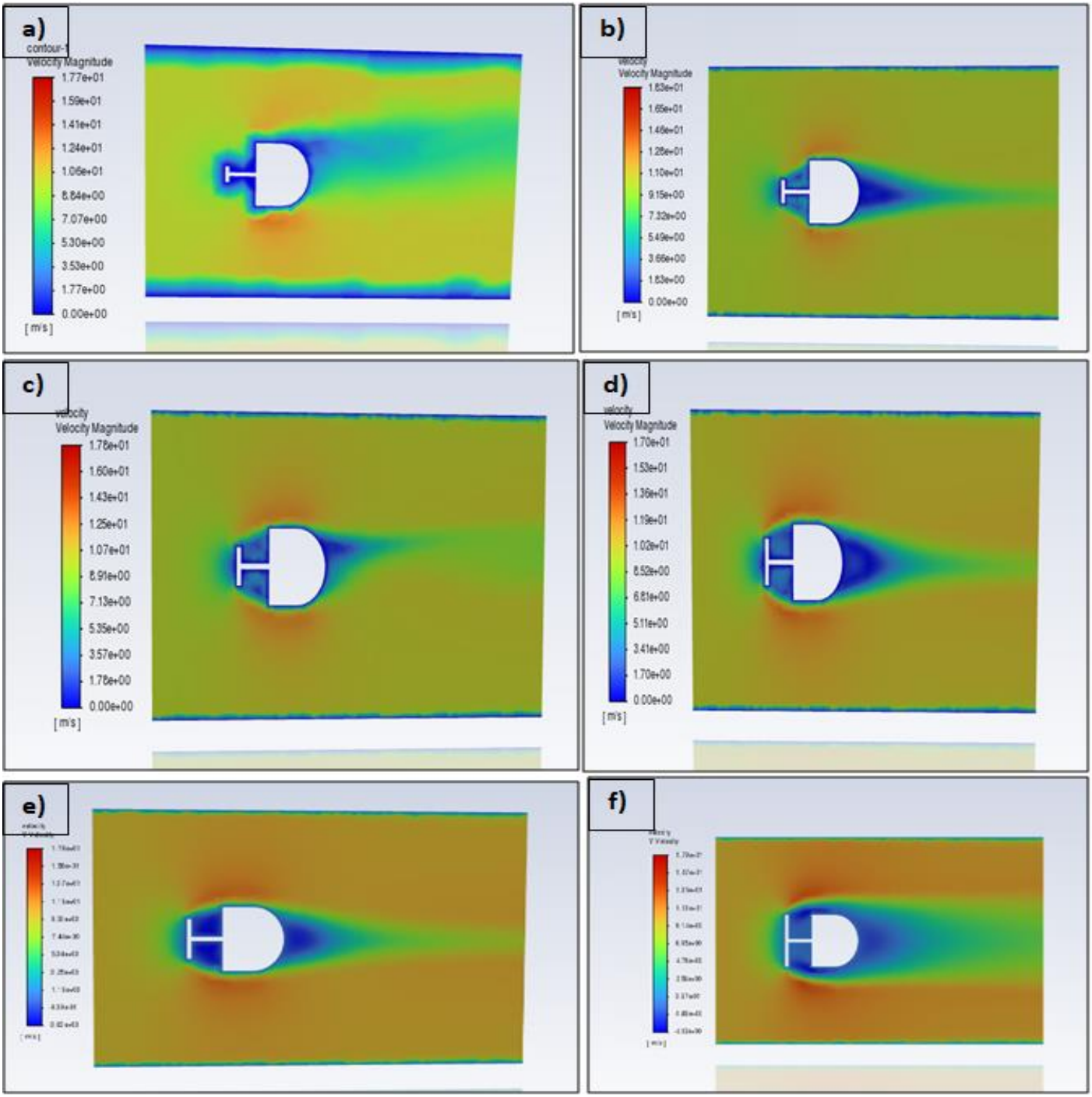

Fig 8 The velocity stream of various width ratios (b/lb2): 0.25, 0.37, 0.5, 0.62, 0.75, as well as 1.

The variation of the pressure coefficient with the width ratios for a 0.5 gap ratio at a speed value of 15 m/s is represented in Figures 9 (a) through 9 (f). As the combination varies, the pressure distribution seems to be contrasted. A high excess pressure value will affect the rear body face when the width ratio is of small values, such as 0.25 and 0.37. The high pressure is given in the yellow area because the flow stagnates as it is split from the front body and strikes the face. Then, the pressure will be separated from the rear body face and accelerated on the lower and upper rear body sides. Therefore, the pressure will drop to

ISSN No:-2456-2165

reach negative values in Figures 9 (a) and 6 (b) in the blue area.

A low-pressure coefficient will affect the rear body when the width ratios are 0.5 and 0.62, defined in the blue area. On the other hand, the front body face experience a high-pressure coefficient. These results are represented in Figures 9 (c) and 9 (d). The comparison between these results and the optimum case is represented in Figure 9 (e), in which the front face of the rear body experiences low-pressure values in the blue area. However, low-pressure values are applied on the lower and upper surfaces. The boundary layers term might be used for interpreting these results as the leading edges of the front body are re-attached with the front face corners of the rear body. Then, a small wake zone will be produced behind the rear body. Accordingly, the drag coefficient will be lowered.

The large ratio of width (b1/b2) when equals 1.0, there will be a high value of the positive pressure (+Cp) on the front-body face, whereas there will be a negative pressure value for the entire rear body, as represented in Figure 9 (f). As a result, the drag coefficient is higher than the rear body alone.

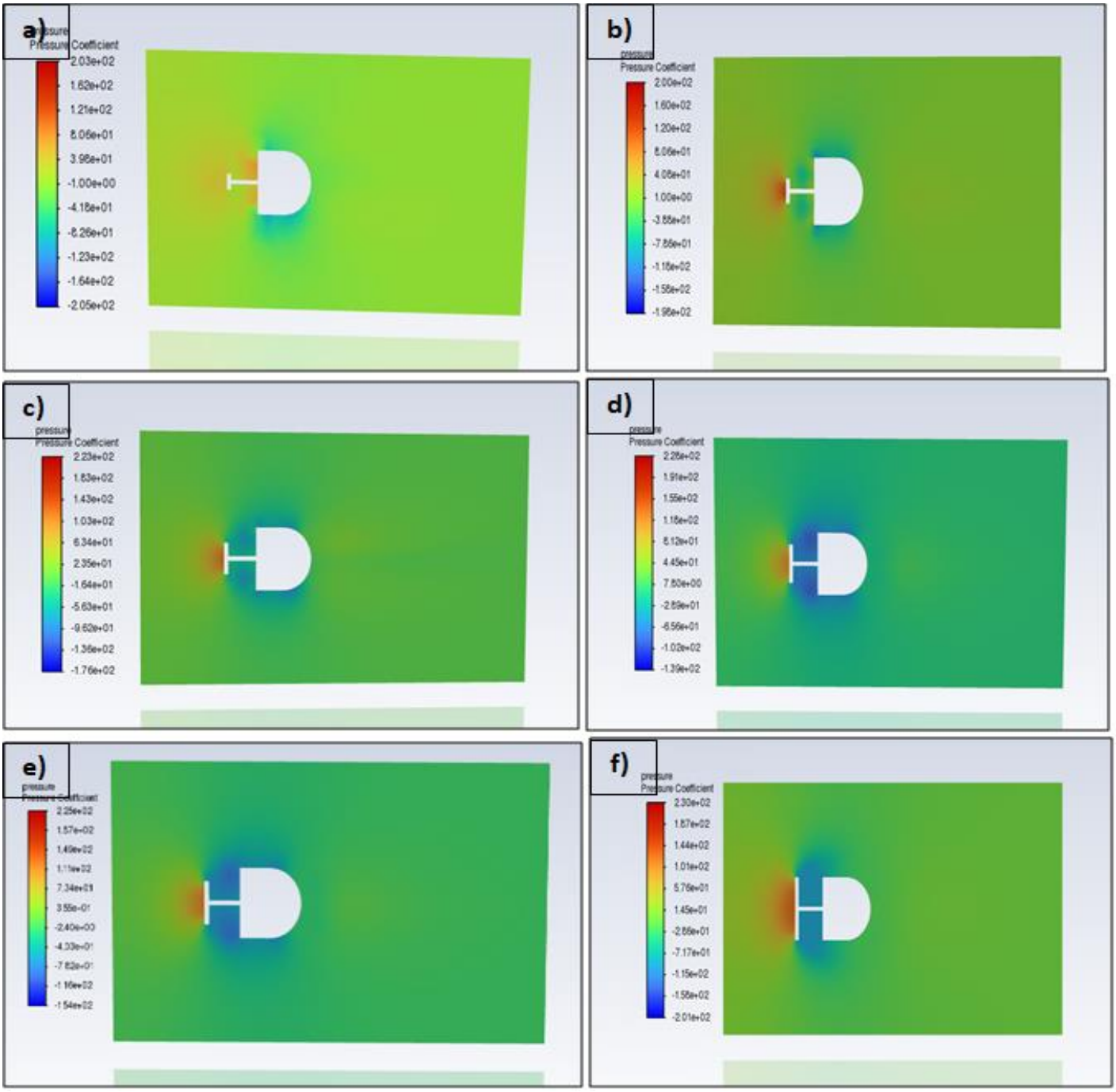

Fig 9 The Pressure Distribution of Various Width Ratios (B/Lb2): 0.25, 0.37, 0.5, 0.62, 0.75, as Well as 1

The discrepancy of the drag-coefficients (CD/CD0) is plotted regarding each combination with a gab-ratio in Figure 10 (a) through Figure 10 (f) for Reynold number range from 1*105-1. 8*105. As shown, the trend in the ratio

ISSN No:-2456-2165

of drag coefficients is like a width ratio ($\frac{b1}{b2}$=0.25, and $\frac{b1}{b2}$ = 0.37), as represented in Figure 10 (a) and Figure 10(b), which represents decreasing in the drag-coefficient ratio as the gap ratio increasing.

The explanations for this trend are related to separation in the layer boundaries, which tends to re-attach the rear body corners. The optimum combination of ($\frac{b1*}{b2}$=0.75, $\frac{g*}{b2}$=0.5) is represented in Figure 10 (e). The effect of optimum shielding, which happens in a certain combination, in addition to the separation in the layers boundary from the front body, is close to the rear edges of the leading body.

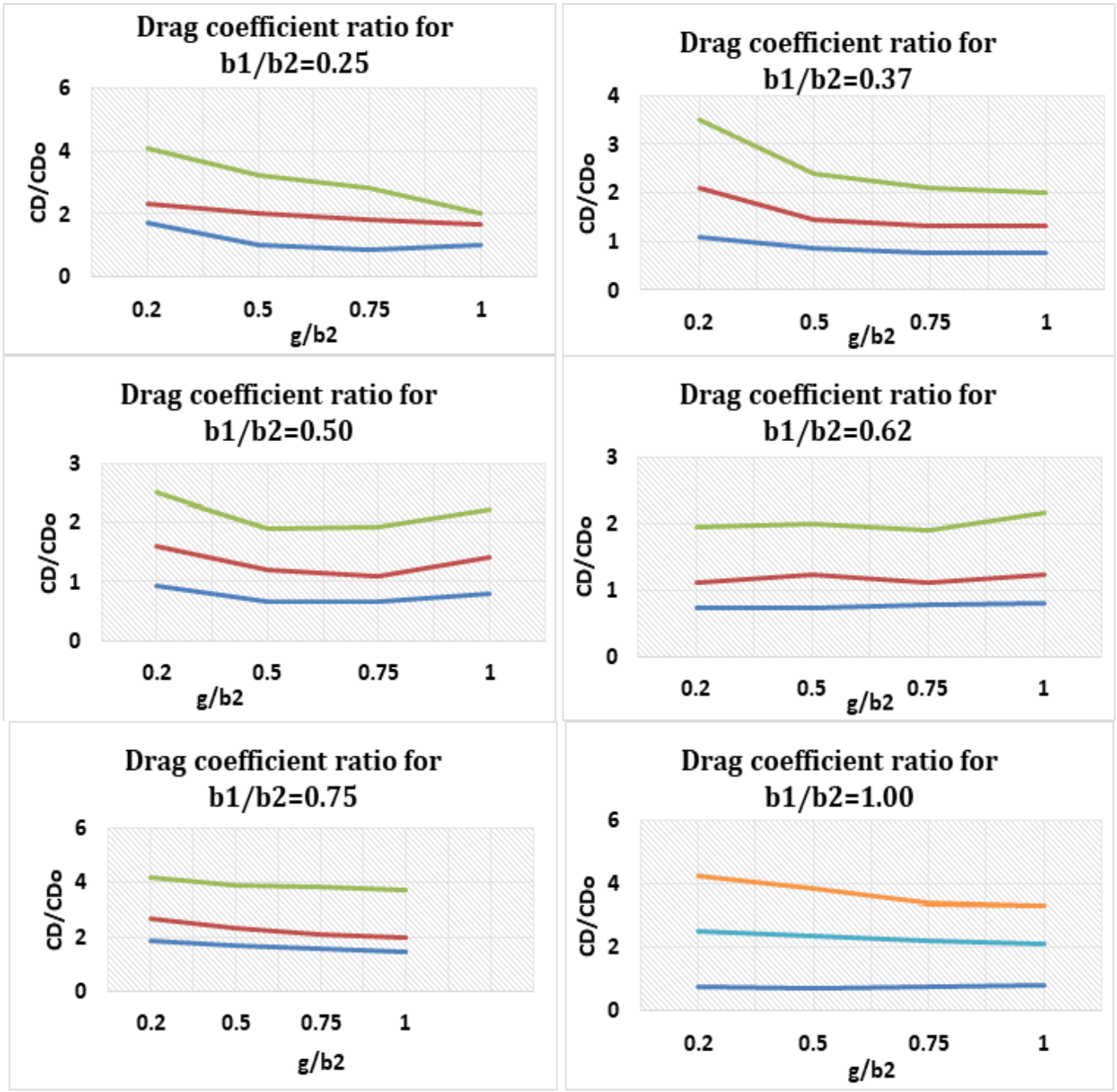

Fig 10 The Drag Coefficient Ratio when B1/B2 = 0.25, 0.37, 0.50, 0.62, 0.75, as Well as 1 with Various Velocities

The contour components of the stream velocity for optimum and specific width ratio ($\frac{b_1^*}{b_2}$ equals 0.75, with varying gap ratios ($\frac{g}{b_2}$ equals 0.25, 0.5, 0.75, and 1.0) as shown in Figures 11 (a), (b), (c), and (d), respectively. The wake zone, which is located next to the optimum combination, has a small size and steadier combination, as represented in Figure 11 (c) when compared with Figure 10 (a), (b), and (d), respectively. This behavior is attributed to the effect of shielding.

ISSN No:-2456-2165

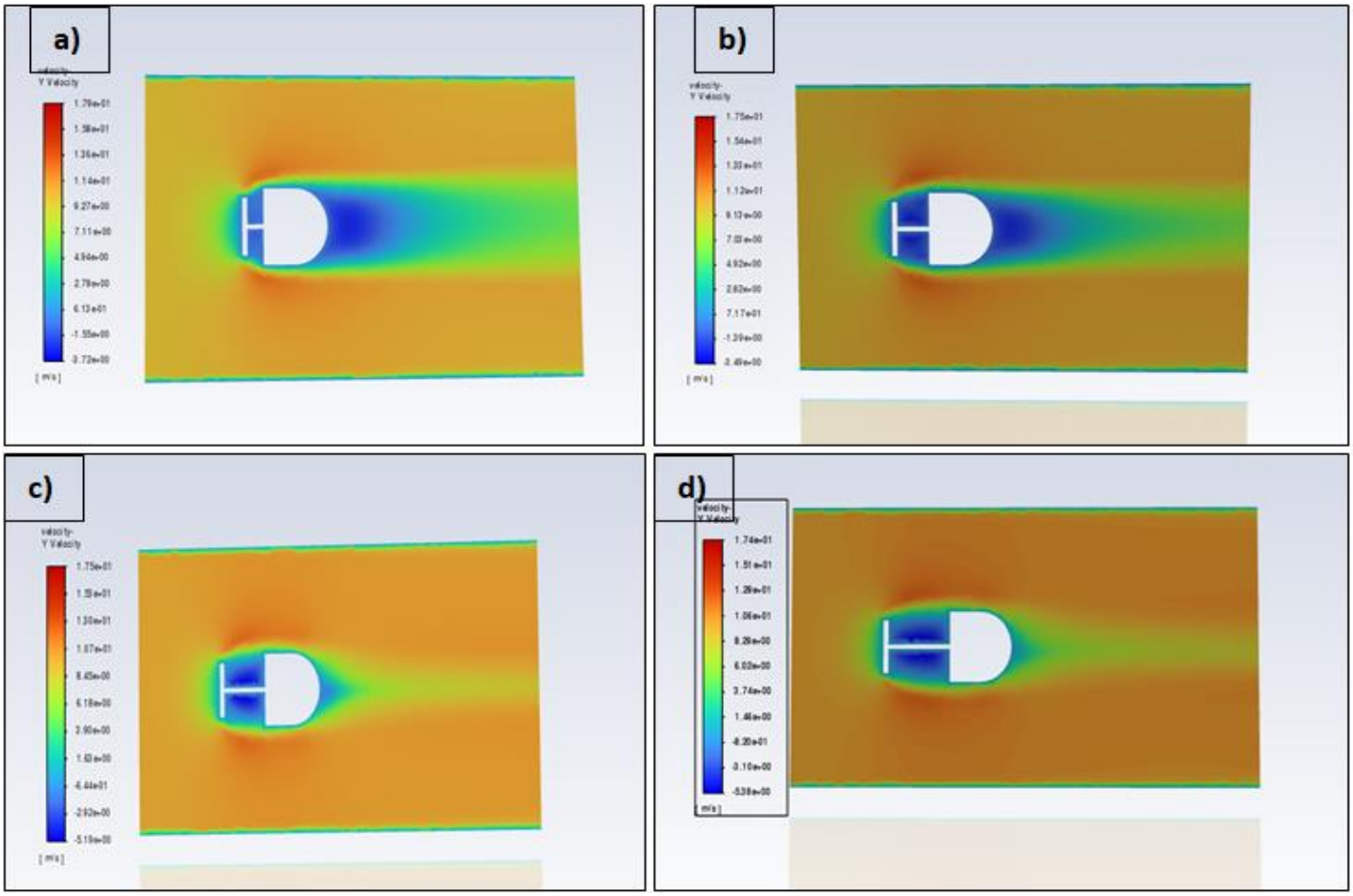

Fig 11 The Components of flow Stream Velocity for Various Width Ratios (B/Lb2): 0.75, with Various Gap Ratios 0.25, 0.50, 0.75 (G/B2), as Well as Velocity is 15 M/S.

A width ratio of (b_1 / b_2) represents the drag reduction percentage in Figure 12 for several velocities. The showed behavior is similar to the velocities that were simulated. The maximum possible reduction in the coefficient of the aerodynamic could be achieved with a relatively optimal combination of ($\frac{g^*}{b_2} = 0.5$ and $\frac{{b_1}^*}{b_2} = 0.75$) at a specific velocity of V=15m/s. When the other optimal configurations are compared, it was found that 75% more than the percentage when the velocity is 20 m/s.

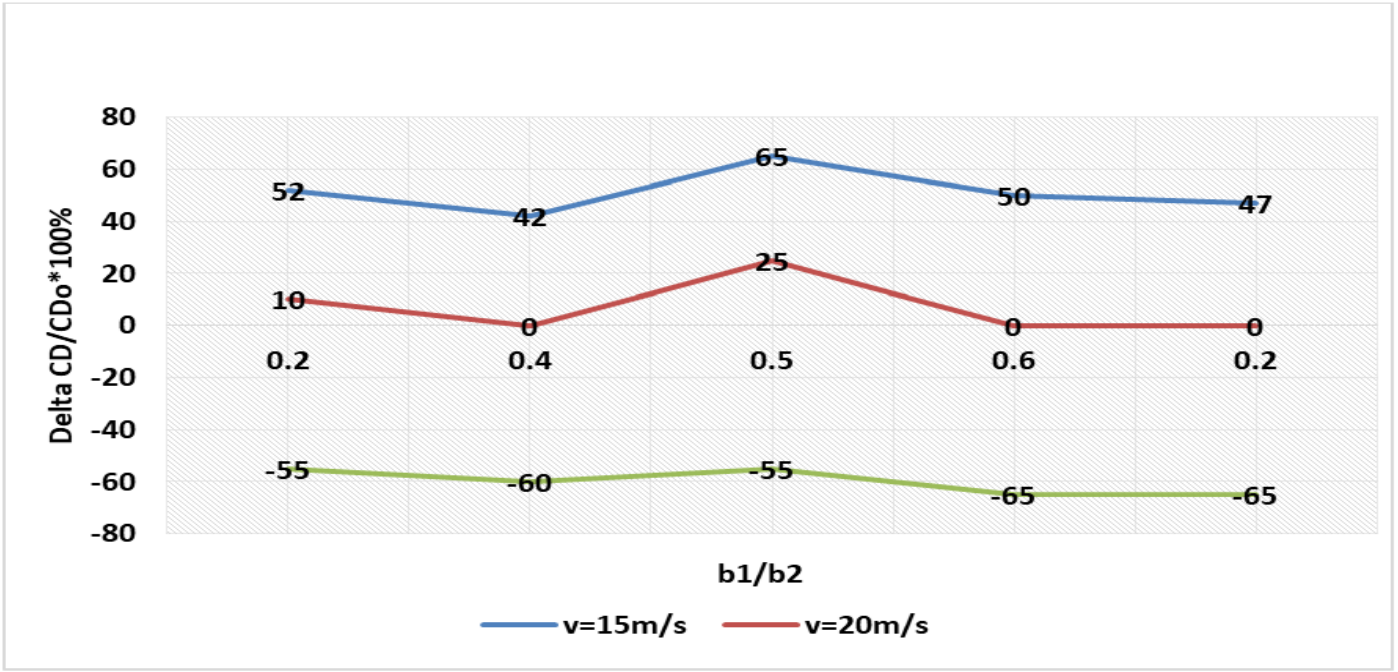

Fig 12 The Variation in Drag Reduction Percentage for Different Velocities

However, based on the previous outcomes, it was shown that a considered drag reduction had been found for a specific configuration. Several cases can be found other than the optimal outcomes with lower drag reduction. This could be attributed to the separate layers from the square plate (front body).

The numerical results have been evaluated for the optimal coefficient of dragging (C_D) found for the corresponding variation in the velocity. Moreover, the numerical outcomes regarding the C_D found in this study were compared with the obtained experimental data with a deviation of about 15% when the velocity was relatively low ($V = 15\ \frac{m}{s}$).

IV. CONCLUSION

This paper concludes and analyses the proposed model of three-dimensional CFD simulation outcomes, incompressible and unsteady flow roughly the back body, and various geometrical combinations such as gap ratios and width are concerned. The impact of shielding of different square plates positioned coaxially like front side body upstream with a rounded rear body with Reynolds number established on rear body width in the field from 1 to 1.8 that are multiple with 105 that are offered in this paper. Therefore, it is probable to conclude after analyzing the proposed model in ANSYS software. According to the numerical simulation, it was found that the optimal combination was achieved when the ratio of $\frac{b1}{b2}$=0.75 and $\frac{g}{b2}$ =0.5, resulting in a percentage of 48% drag reduction as well as a possible 12% of the speeds of 15-20 m/s. Also, some other combinations that were investigated reduced the drag coefficient by a percentage of (2-10) %, which is considered a low value when compared with the optimal combination drag reduction. Although the obtained values showed a reasonable and considerable drag reduction from the optimal cases, several combinations found a drag more than the rear body, resulting in a negative percentage of drag reduction.

REFERENCES

[1]. Aabid, A. et al., 2021. CFD Analysis of Splitter Plate on Bluff Body. *CFD Letters,* 11(11), p. 25–38.

[2]. Afifi, A., Aabid, A. & Khan, S. A., 2021. Numerical investigation of splitter plate effect on the bluff body using finite volume method . *Materials Today: Proceedings,* Volume 38, pp. 2181-2190.

[3]. Bao, D., Borée, J., Haffner, Y. & Sicot, C., 2022. Near wake interactions and drag increase regimes for a square-back bluff body. *Journal of Fluid Mechanics,* p. 936.

[4]. Chen, W., Ji, C., Alam, M. M. & Xu, D., 2022. Three-dimensional flow past a circular cylinder in proximity to a stationary wall. *Ocean Engineering,* p. 110783.

[5]. Chen, Z., Xu, Y., Huang, H. & Tse, K. T., 2020. Wind tunnel measurement systems for unsteady aerodynamic forces on bluff bodies: review and new perspective. *Sensors,* 20(16), p. 4633.

[6]. Imron, C., Suhariningsih, W. & Basuki, Y., 2013. Numerical simulation of fluid flow around circular and I-shape cylinder in a tandem configuration. *Applied Mathematical Sciences,* Volume 7, pp. 5657-5666.

[7]. Khalid, M. S. & Rathakrishnan , E., 1996. Front Body Effects on Drag and Flow field of a Three-Dimensional Noncircular Cylinder. *AIAA Journal,* 31(7), pp. 1345-1347.

[8]. Konstantinidis, E. & Bouris, D., 2012. Bluff Body Aerodynamics and Wake Control. *Jorge Colman Lerner and Ulfilas Boldes,* Volume 10, pp. 63-78.

[9]. Li, B., Zhang, H., Saranteas, K. & Henson, M. A., 2021. A rigid body dynamics model to predict the combined effects of particle size and shape on pressure filtration. *Separation and Purification Technology,* p. 119462.

[10]. Malizia, F., Montazeri, H., Hespel, P. & Blocken, B., 2016. Numerical simulation of flow around a circular cylinder: comparison of LES and URANS turbulence models. *In Proceedings of the 8th International Colloquium on Bluff Body Aerodynamics and Application.*

[11]. Sajali, M., Aabid, A., Khan, S. A. & Mehaboobali, F. A., 2021. Numerical investigation of flow field of a non-circular cylinder.. *Department of Mechanical Engineering, Faculty of Engineering.*

[12]. Talele, V., Mathew, V. K., Sonawane, N. & Sanap, S., 2021. CFD and ANN approach to predict the flow pattern around the square and rectangular bluff body for high Reynolds number. *Materials Today. Proceedings,* pp. 3177-3185.

[13]. Yagmur, S. et al., 2015. Experimental and numerical investigation of flow structures around cylindrical bluff bodies. *In EPJ Web of Conferences EDP Sciences.,* Volume 92, p. 02113.